Avalanche, Joule Breakdown and Hysteresis in Carbon Nanotube Transistors

Eric Pop*, Sumit Dutta, David Estrada, Albert Liao
Dept. of Electrical & Computer Engineering and Beckman Institute
University of Illinois at Urbana-Champaign
2258 Micro and Nanotechnology Laboratory
208 N. Wright St, Urbana IL 61801, USA
Tel: +1 217 244-2070, *E-mail: epop@illinois.edu

***Abstract*—We explore several aspects of reliability in carbon nanotube transistors, including their physical dependence on diameter. Avalanche behavior is found at high fields (5-10 V/μm), while Joule breakdown is reached at high current and heating, in the presence of oxygen. Finally, we describe a method for minimizing hysteresis effects via pulsed measurements.**

Keywords-carbon nanotube, avalanche, hysteresis, breakdown

I. INTRODUCTION

Carbon nanotubes (CNTs) are quasi-one-dimensional conductors with excellent electron mobility (10-20x higher than silicon) [1] and lattice thermal conductivity (comparable to that of diamond) [2]. This has prompted their use as either circuit elements, such as transistors or interconnects, or as thermal heat sink components. In all such uses, nanotubes can undergo operation under high electric field or temperature gradients, both of which raise fundamental questions about the reliability and endurance of CNTs under such stress.

In this paper, we present several recent results regarding single-wall CNT behavior at high electric fields and elevated temperatures. We investigate avalanche breakdown in semiconducting CNTs and Joule breakdown in metallic CNTs. We also examine the effects of dielectric charge trapping on the electronic properties of nanotube devices via pulsed measurements which minimize the hysteresis typically noted during DC sweeps.

II. AVALANCHE BREAKDOWN

The typical CNT devices used in our studies are shown in Fig. 1. These are grown by chemical vapor deposition (CVD) from a patterned Fe catalyst island on t_{OX} = 100 nm thermal SiO_2 and highly p-doped Si wafers which also serve as back gates. The nanotubes are contacted by evaporating 40 nm of Pd followed by lift-off, as shown in Figs. 1A and 1C. A nominally 0.5 nm Ti layer is centered below the large pad area (100x250 μm) for better electrode adhesion, although this does not extend to the edge region and the nanotube contacts themselves. The Pd edge electrode allows for typically Ohmic behavior, with contact resistance R_C ~ 30-50 kΩ, estimated from low-field I_D-V_{DS} measurements at high back gate voltage $|V_{GS}|$. Metallic and semiconducting nanotubes were sorted by their on/off ratios, measuring current (I_D) vs. gate-source voltage (V_{GS}), as in Fig. 1B. As-grown devices show unipolar p-type behavior with negative threshold voltage (V_T). Dimensions were obtained by atomic force microscopy (AFM), indicating typical diameters in the range d ~ 2–3.6 nm.

Current vs. drain-source voltage (V_{DS}) measurements were made in air and vacuum. Metallic CNTs saturate from self-heating and strong electron-phonon scattering [3] up to Joule breakdown. By contrast, most semiconducting tubes turned on at large $|V_{GS}|$ exhibit a sharp current increase at high VDS, due to avalanche impact ionization (II) and free electron-hole pair (EHP) creation, as shown in Figs. 2B and 3A. Measurements carried out in vacuum (~10^{-5} Torr) allow study of the avalanche without breaking the nanotubes by oxidation. It is important to note that devices were typically measured in the reverse bias regime, with $V_{GS} < 0 < V_{DS}$ and $|V_{GS}| > |V_{DS}|$. By contrast, in Schottky mid-gap contacted devices, the ambipolar regime $V_{DS} < V_{GS} < 0$ "splits" the potential drop along the nanotube result-

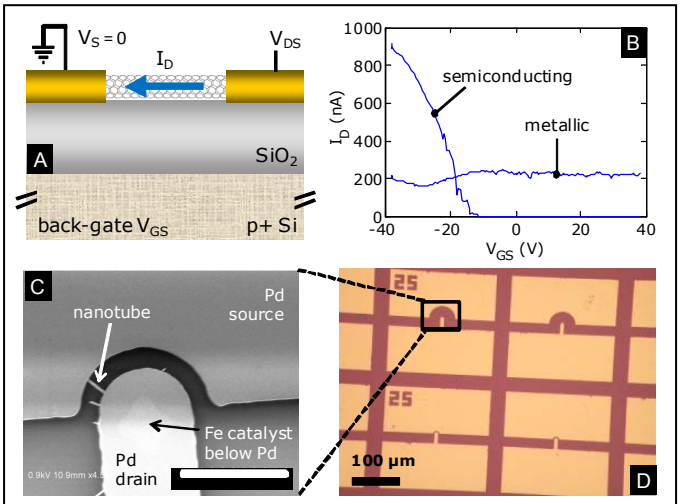

Fig. 1: (A) Typical back-gated nanotube device used in this study. (B) Back-gate voltage dependence, distinguishing semiconducting from metallic nanotubes. (C) Scanning electron micrograph (SEM) image of nanotube device. Semi-circular electrodes are used for better control over channel length (scale bar 10 μm). (D) Optical image of several fabricated devices, showing Ti/Pd pad dimensions.

This work has been supported in part by NASA-KSC and by the Nanoelectronics Research Initiative (NRI) through the MIND center.

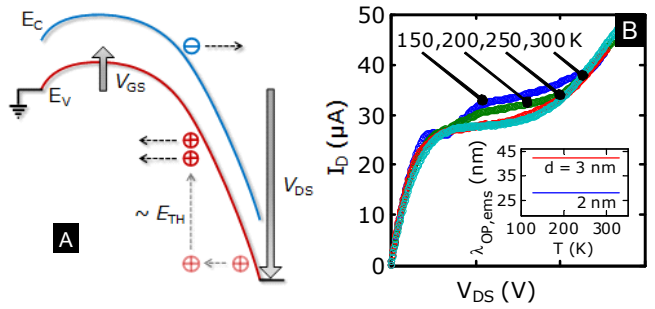

Fig. 2: (A) Schematic band diagram and EHP generation under avalanche and reverse bias conditions.. (B) Temperature insensitivity of impact ionization tail. Measured reverse bias I_D-V_{DS} curves for a CNT with d ~ 2.2 nm and L ~ 2.2 μm, in vacuum. There is little temperature dependence of the avalanche tail unlike, e.g., impact ionization in bulk silicon. This is attributed to the very small temperature dependence of the band gap and the optical phonon emission mean free path in nanotubes ($\lambda_{OP,ems}$ calculated for two diameters, following Ref. [3] in the inset).

ing in lower longitudinal electric fields and transport by both electrons and holes. In the reverse bias regime, holes are the majority carriers in our CNTs until the avalanche mechanism partially turns on the conduction band (Fig. 2A).

We have described the details of the avalanche process in CNTs and its features in Ref. [4]. By contrast to avalanche in many semiconductors (such as silicon), avalanche in CNTs is largely temperature-independent, as shown in Fig. 2B. In silicon, as the phonon scattering rate increases with temperature, free carriers gain less energy from the field and the avalanche rate decreases at higher temperatures. In CNTs we observe negligible temperature dependence of the impact ionization region at high drain bias. The essential difference lies in that the optical phonon (OP) emission mean free path (MFP) $\lambda_{OP,ems}$ varies minimally with temperature in CNTs, because the OP energy (~0.2 eV) is much greater than in other materials. This MFP is calculated and shown for two diameters as the inset to Fig. 2B. The lack of temperature dependence and that of a Joule heating dependence of the avalanche also indicates there is no significant contribution from thermal current generation. Quite the opposite, given the generation of electron-hole pairs (EHPs) rather than OPs during avalanche, a slightly lowered Joule heating rate in the highest field region near the drain is expected.

In a simple physical model [4] the avalanche impact ionization (II) current can be written $I_{II} \approx I_S \exp(-E_{TH}/q\lambda_{OP,ems}F)$, where I_S is the saturation current reached before II becomes significant. Inserting the expected diameter dependence $E_{TH} \approx E_1/d$ and $\lambda_{OP,ems} \approx \lambda_1 d$, we can find the average field at which avalanche becomes significant, $\langle F_{TH} \rangle \approx E_1/q\lambda_1 d^2 \ln(2)$. The experimental data can be used to extract this field (but not the peak field) in a nanotube device, which is plotted vs. $1/d^2$ for nanotubes of several diameters in Fig. 3B. The slope of the linear fit thus scales as the ratio between the avalanche threshold energy and the inelastic MFP, E_1/λ_1. However, the avalanche process is a strong function of the field, and most EHPs are generated at the peak field, $F_{TH,MAX}$. The latter is estimated by noting that the potential near the drain has a dependence $V(x) \approx \ell F_0 \sinh(x/\ell)$, where $F_0 \sim 1$ V/μm is the saturation velocity field and ℓ is an electrostatic length scale comparable to t_{OX}. Fitting this expression to our voltage conditions and nanotube dimensions, we find $F_{TH,MAX}/\langle F_{TH} \rangle \approx 4.5$ for L = 1 μm device, and 3.5 for L = 2 μm. Thus, using the peak instead of the average field, the empirically extracted slope gives $E_1/\lambda_1 \sim 0.088$ eV·nm, where we take $E_1 = 1.26$ eV as the bottom of the third sub-band. Accounting for fit errors, this yields $\lambda_1 = 15 \pm 3$ nm as the inelastic OP emission MFP for d = 1 nm, or generally $\lambda_{OP,ems} = \lambda_1 d$. This value is in good agreement with the theoretically predicted 14d nm in Ref. [5], and our approach demonstrates an additional, novel empirical method for extracting this important transport parameter from high-field electrical measurements.

III. Joule Breakdown

Pushing both semiconducting and metallic nanotubes to very high drain voltages *in air* leads to significant Joule heating and breakdown by oxidation. This approach can be used to understand high-temperature and high-voltage stress effects on CNT device properties, since the burn-out temperature of nanotubes is typically known to be $T_{BD} \sim 600\ ^oC$ [6].

Recently, we have studied in-air electrical breakdown characteristics of substrate-supported single-wall carbon nanotubes [6]. Several published data sets were analyzed, spanning a wide range of nanotube diameters, lengths and contact properties. Nevertheless, a few simple, universal scaling rules were found

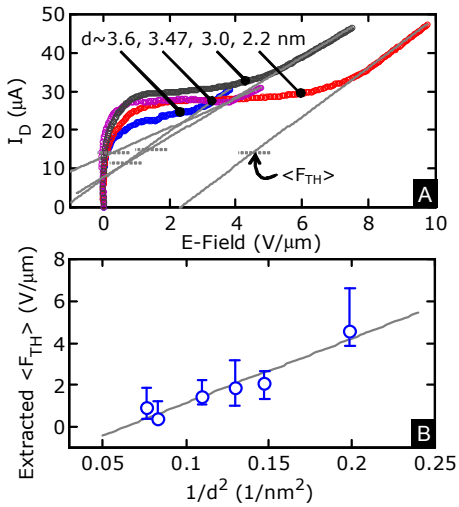

Fig. 3: Diameter dependence of avalanche threshold field, F_{TH}. (A) Current vs. average channel field (V_{DS}-$I_D R_C$)/L for several CNT diameters and lengths between 2.2-4.1 μm. The avalanche threshold is extrapolated from the tail region and defined as the field $\langle F_{TH} \rangle$ at which the current reaches one half the saturation value. (B) Extracted average $\langle F_{TH} \rangle$ vs. $1/d^2$. The uncertainty in diameter from AFM measurements is 0.4 nm. The slope of the linear fit scales as the ratio between the avalanche energy threshold and the inelastic OP emission length, $E_{TH}/\lambda_{OP,ems}$. Taking $E_{TH} \sim 1.26/d$ eV, the OP emission length is found to be ~15d nm [4].

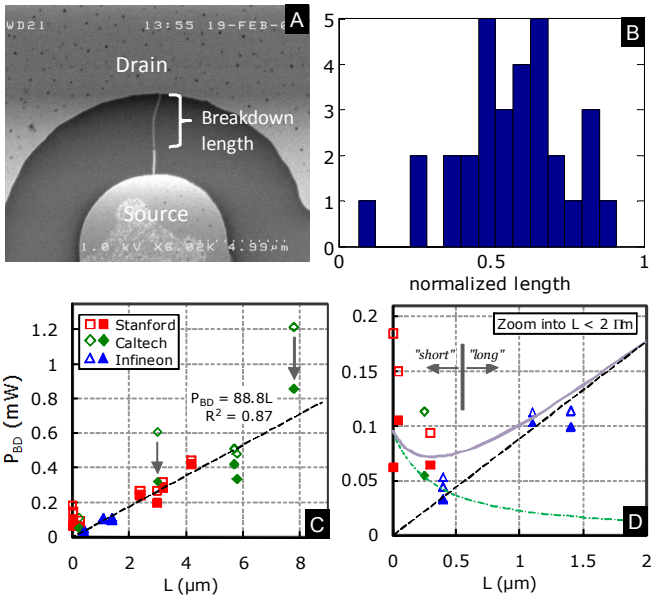

Fig. 3: (A) SEM image showing CNT breakdown location after high voltage stress and Joule breakdown (B) Distribution of breakdown location normalized by CNT length, illustrating typical break near the middle, consistent with Joule heating. (C) Breakdown power vs. CNT length from several data sets [6]. Empty symbols are before, and solid symbols are after removing the contact power dissipation I^2R_C (arrows highlight some of the changes). (D) Same data sets, zoomed into the shorter nanotube range. Lines are several thermal dissipation models described in [6]. The finite breakdown power at near-zero length cannot be reproduced without including the CNT-electrode contact thermal resistance R_T.

to emerge, showing that the breakdown power of long nanotubes scales linearly with their length (electrode separation), whereas the breakdown of very short nanotubes is almost entirely limited by their contact resistance. The data and models are shown in Figs. 3C and 3D. A minimum in the electrical power required to break single-wall carbon nanotubes is found (~0.05 mW), which may be tailored through careful contact (resistance) engineering.

Two length limits appear to characterize Joule breakdown of CNTs, with respect to twice the thermal healing length along the nanotube ($2L_H$ ~ 0.5 μm). For "long" CNTs, Joule breakdown is limited by heat dissipation into the SiO_2 substrate, such that the power at breakdown $P_{BD} \approx g(T_{BD}-T_0)L$, where g is the heat conductance into the substrate per unit length, T_0 is the ambient temperature and L the nanotube length [6]. A simple fit to the experimental data reveals $g \approx 0.15$ $Wm^{-1}K^{-1}$. For "short" CNTs, Joule breakdown is limited by heat dissipation at the contacts, and $P_{BD} \approx (T_{BD}-T_0)/(L/8kA+R_T/2)$ where k is the thermal conductivity along the CNT, A is its cross-sectional area, and R_T is the thermal resistance at the contacts. A simple fitting model reveals that a typical value for the CNT-Pd electrode contacts is $R_T \approx 1.2 \times 10^7$ K/W [6].

A further study of the breakdown *location* in several CNT devices is consistent with the Joule heating mechanism. Figs. 3A and 3B reveal the location of the breaking point imaged by SEM across several CNT devices. Assuming uniform heating in the CNT and symmetric (left/right) heat dissipation, the simple thermal models predict the maximum temperature to occur at the middle of the nanotube. An experimental histogram of the breakdown point reveals a consistent picture in Fig. 3B. The spread in breakdown location is attributed to asymmetric thermal or electrical contact resistance (left vs. right electrode), as well as possible defects along the CNTs. Nevertheless, the histogram supports the simple thermal Joule breakdown model, while prompting further study to understand the role of diameter, defects, substrate, and contacts on Joule breakdown.

IV. Hysteresis

CNT transistors are often back-gated, with the nanotube resting on SiO_2 and exposed to the ambient environment. Hysteretic behavior in the transfer characteristics (I_{DS}-V_{GS}) is common, and varies depending on sweep direction, sweep rate, and environmental conditions, as shown in Fig. 4. This is typically attributed to charge trapping by surrounding water molecules and to charge injection into the substrate [7,8]. Thus, it is often unclear which electrical characteristics should be used to extract carrier mobility and threshold voltage, lead-

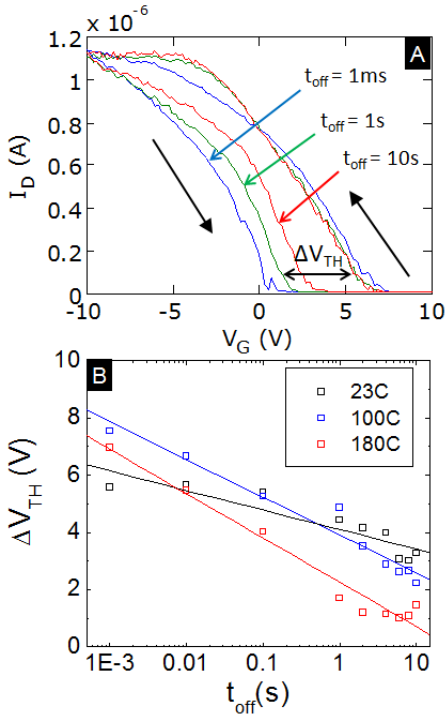

Fig. 4: (A) Typical transfer curve of a back-gated CNT transistor at room temperature. A threshold voltage hysteresis usually exists between the forward and backward sweep (with black arrows). However, the magnitude of the hysteresis decreases during pulsed measurements with the pulse OFF time. (B) Voltage hysteresis gap (ΔV_{TH}) for three different temperatures and a range of pulse OFF times. The magnitude of the hysteresis decreases with high t_{OFF} for all temperatures, but the rate of decrease is fastest at 180 °C. (C) Hysteresis vs. CNT diameter and length (inset). A linear increase is seen with CNT diameter, consistent with larger density of states, and increased charge injection into the substrate [10].

ing to large discrepancies (>10x) in reported values as both the forward [1] and backward [9] I-V sweeps have been used. Pulsed measurement techniques have been show to suppress hysteresis in CNT transfer characteristics [10]. As hysteresis is reduced, both forward and backward sweeps move towards a common, unique central transfer characteristic which reveals the "true" device mobility.

In this study, we measured CNT transfer characteristics using a Keithley 2612 dual-channel system source-meter over a gate voltage sweep range of -10 to 10 V, with V_{DS} = 50 mV. The gate voltage pulse width and duty cycle were varied over a wide range (1 ms – 10 s). All measurements were made in air, at ambient temperatures from 23 – 180 ^{o}C. We define the hysteresis gap as the difference in threshold voltage between the forward and backward sweeps (ΔV_{TH}), as determined by the linear extrapolation method. While we do not find a significant dependence of hysteresis on the pulse ON-time (varied over a range of 250 µs – 1 ms) we do find a significant dependence of hysteresis on the pulse OFF time.

Fig. 4 illustrates typical results for our devices; the magnitude of the hysteresis is shown to decrease with increased OFF time. It is also interesting to note that both the forward and the backward sweeps move towards a central transfer characteristic. Fig. 4B shows the dependence of hysteresis as a function of both pulse OFF time and temperature. We find greater reduction in hysteresis at higher temperatures (≈2x at 180°C), where water has been more effectively desorbed from the nanotube/SiO_2 surface. With long OFF (delay) times between pulses, the hysteresis is nearly removed, indicating the very large relaxation time of surface traps surrounding the CNT.

Fig. 5 shows the dependence of hysteresis on nanotube diameter and length (inset). We do not find a dependence of hysteresis on CNT length but we find an approximately linear scaling with nanotube diameter. This suggests the amount of environmental injected and trapped charge is directly proportional to the density of states, and the total charge in the nanotubes. This confirms the similar conclusion reached by Ref. [10] through a different argument, which noted the temperature dependence of the hysteresis is the same as that of the total nanotube charge.

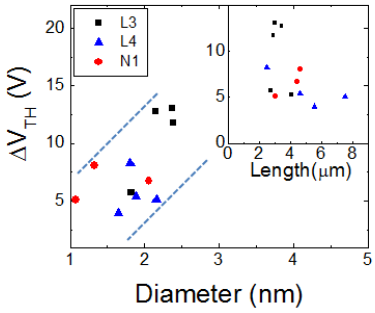

Fig. 5: Hysteresis vs. CNT diameter and length (inset). A linear increase is seen with CNT diameter, consistent with larger density of states, and increased charge injection into the substrate.

SUMMARY

We have investigated and described several reliability concerns regarding metallic and semiconducting single-wall carbon nanotubes (CNTs). In particular, avalanche breakdown in semiconducting CNTs has been recently studied for the first time, and found to occur at relatively low threshold fields (~5 V/µm) and have negligible temperature dependence compared to typical semiconductors. The high-bias measurements in the avalanche regime can also be used to extract an approximate value for the inelastic optical phonon scattering length in CNTs, itself an essential transport parameter (λ_{OP} ~ 15d, where d is the CNT diameter). We note avalanche is not observed in metallic CNTs due to the absence of a band gap.

Applying voltages beyond avalanche leads to significant Joule heating and eventual breakdown in CNTs. By examining several data sets we find simple models for breakdown power scaling, providing an intuitive, physical understanding of the breakdown process. The electrical and thermal resistance at the electrode contacts limit the breakdown behavior for submicron SWNTs, the breakdown power scales linearly with length for microns-long tubes, and a minimum breakdown power (~0.05 mW) is observed for the intermediate (~0.5 µm) length range.

Finally, we examine the long-standing issue of hysteresis in semiconducting CNTs, and uncover its diameter and pulse OFF-time dependence. In particular, at elevated temperatures (180 ^{o}C) and long pulse delays (10 s) the hysteresis gap is usually eliminated, and the transfer characteristics unite towards a "true" common curve, unique to each CNT device.

ACKNOWLEDGMENT

We acknowledge valuable discussions with D. Jena, M. Kuroda, J.-P. Leburton, J. Lyding, C. Richter and Y. Zhao.

REFERENCES

[1] X. Zhou et al, *Phys. Rev. Lett.* 95, 146805 (2005).
[2] E. Pop et al, *Nano Lett.* 6, 96 (2006).
[3] E. Pop et al, *J. Appl. Phys.* 101, 093710 (2007).
[4] A. Liao et al, *Phys. Rev. Lett.* 101, 256804 (2008).
[5] V. Perebeinos and P. Avouris, *Phys. Rev. B* 74, 121410(R) (2006).
[6] E. Pop, *Nanotechnology* 19, 295202 (2008).
[7] W. Kim et al, *Nano Lett.* 3, 193 (2003).
[8] A. Vijayaraghavan et al, *Appl. Phys. Lett.* 89, 162108 (2006).
[9] T. Durkop et al, *Nano Lett.* 4, 35 (2004).
[10] H. Lin and S. Tiwari, *Appl. Phys. Lett.* 89, 3 (2006).